# Optical sorting of small chiral particles by tightly focused vector beams

Manman Li,[1] Shaohui Yan,[1] Yanan Zhang,[1,2] Yansheng Liang,[1] Peng Zhang,[1] and Baoli Yao[1,*]

[1]*State Key Laboratory of Transient Optics and Photonics, Xi'an Institute of Optics and Precision Mechanics, Chinese Academy of Sciences, Xi'an 710119, China*

[2]*University of Chinese Academy of Sciences, Beijing 100049, China*

(Received 14 November 2018; published 12 March 2019)

The identification and separation of substances by chirality has always been an important problem in biomedical research and industry. Light beams carry optical momentum, and can exert optical force on any object they impinge due to the transfer of momentum. Different chiral objects will experience different optical forces when illuminated by the same light beam. We demonstrate here, based on the dipolar approximation, that a tightly focused vector beam can selectively trap and rotate small chiral particles in the transverse plane via the chirality-tailored optical forces. The radial optical force can transversely trap the chiral particles off axis or push them away depending on the real part of the chirality parameter, while the lateral optical force manifesting as the azimuthal optical force can drive the trapped particles to orbitally rotate with opposite chiral absorption in opposite directions. The study reported here may find applications in discriminating and separating chiral objects with specified chirality.

DOI: 10.1103/PhysRevA.99.033825

## I. INTRODUCTION

Chirality, derived from the Greek $\chi\varepsilon\iota\rho$ (*kheir*), "hand," refers to an asymmetry that an object cannot be superposed onto its mirror image by any rotation or translation [1]. As an intrinsic property, chiral objects abound in nature and the human hand is perhaps the most classic example. In biomedicine, the chirality of a molecule is strongly associated with the biological function. The two mirror images of a chiral molecule can have remarkably different bioactivities and biotoxicities [2]. For example, a chiral protein will become toxic to cells when its original chirality is varied, which may cause many diseases such as Parkinson's, Alzheimer's, type II diabetes, and Huntington's [3]. Therefore, identifying and separating substances by chirality have always been the hot topic in research and industry, especially in pharmaceuticals and agrochemicals [4–6].

In recent years, optical sorting of the chiral objects has attracted significant interest for its less invasive and more efficient alternative to the chemical means [7–16]. Different chiral objects tend to interact differently with light beams having the same intensity and polarization. The chiral light-matter interactions involve the cross coupling between electric and magnetic characteristics, resulting in new types of optical forces such as a lateral optical force which acts in the direction with vanishing intensity gradient and energy flow [17–22]. Wang and Chan showed an electromagnetic plane wave can induce a lateral optical force on a chiral particle near a substrate [17]; Hayat *et al.* predicted the transverse spin angular momentum (SAM) density of evanescent waves can give rise to lateral optical forces on chiral particles [19]; Zhang *et al.* demonstrated how to take advantage of interference fields to induce lateral optical forces on chiral particles [22]. Such lateral optical force can push the chiral particles with opposite handedness in opposite directions, facilitating the development of the optical sorting of chiral particles. However, these studies on the optical chirality sorting mainly involved nonparaxial beams with linear or circular polarization state [7–22], and majority situations only consider the case where the chirality parameter takes real values [7–9,11–22].

In this paper, based on the vectorial diffraction method and the dipole approximation model, we demonstrate an approach to separating chiral particles by using not only the lateral optical force but also a radial optical force induced by a tightly focused vector beam composed of radial and azimuthal components and with a $\pi/2$ phase difference between the two components. The effects of different chirality parameters, e.g., imaginary and complex values, on the transverse optical forces are presented. Furthermore, the physical origins of the optical forces are investigated by using the analytical theory. It is shown that the focused vector field can transversely trap the particles on a circle near the intensity maximum, or push them away in a nontrap state, or drive them to orbitally rotate around the optical axis; these are strongly dependent on the particle chirality. These investigations may provide the possibility of identifying and separating chiral particles.

## II. THEORETICAL MODEL

### A. Optical force on dipolar chiral particles

Considering an isotropic chiral particle with relative electric permittivity $\varepsilon_2$ and relative magnetic permeability $\mu_2$ the constitutive relations that connect the complex displacement field **D** and magnetic field **B** to the electric field **E** and magnetization field **H** can be described by [23–25]

$$\begin{bmatrix}\mathbf{D}\\ \mathbf{B}\end{bmatrix}=\begin{bmatrix}\varepsilon_2\varepsilon_0 & i\kappa/c\\ -i\kappa/c & \mu_2\mu_0\end{bmatrix}\begin{bmatrix}\mathbf{E}\\ \mathbf{H}\end{bmatrix}, \tag{1}$$

*yaobl@opt.ac.cn

 

where $\varepsilon_0$, $\mu_0$, and $c$ are, separately, the permittivity, permeability, and the speed of light in vacuum; $\kappa$ is the chirality parameter which is controlled by the inequality $\kappa^2 < \varepsilon_2\mu_2$ [25,26], and is used to describe the chirality of the object. In such chiral medium, there exist two kinds of waves, $k_\pm = k_0[(\varepsilon_2\mu_2)^{1/2} \pm \kappa]$, with $k_0$ being the wave number in vacuum, which corresponds to left- and right-handed circular polarization states. The real and imaginary parts of the chirality parameter $\kappa$ are associated with optical rotation and circular dichroism, respectively [27,28].

When light is scattered by a particle, the transfer of optical momentum from light to particle induces an optical force on the particle. For a spherical dipolar particle with a radius $a$ being much smaller than the trapping wavelength, the optical force can be obtained analytically within the dipole approximation. In a background medium with the relative permittivity $\varepsilon_1$ and permeability $\mu_1$, the vector expression of the optical force can be expressed as [29–31]

$$\langle \mathbf{F} \rangle = \frac{1}{2}\mathrm{Re}\left[\mathbf{p}\cdot(\nabla \mathbf{E}^*) + \mathbf{m}\cdot(\nabla \mathbf{H}^*) - \frac{ck_1^4}{6\pi}\frac{1}{\sqrt{\varepsilon_1\mu_1}}(\mathbf{p}\times\mathbf{m}^*)\right]. \tag{2}$$

Here $k_1 = n_1\omega/c$ is the wave number with $\omega$ being the angular frequency of light and $n_1 = (\varepsilon_1\mu_1)^{1/2}$ being the refractive index of the medium; $\mathbf{p}$ and $\mathbf{m}$ are the induced electric and magnetic dipole moments, which can be written as [25]

$$\begin{bmatrix}\mathbf{p}\\ \mathbf{m}\end{bmatrix} = \begin{bmatrix}\alpha_{ee} & i\alpha_{em}\\ -i\alpha_{em} & \alpha_{mm}\end{bmatrix}\begin{bmatrix}\mathbf{E}\\ \mathbf{H}\end{bmatrix}, \tag{3}$$

with $a_{ee}$, $a_{mm}$, and $a_{em}$ being, separately, the electric, magnetic, and chiral polarizabilities of the chiral particle. Polarizabilities $a_{ee}$, $a_{mm}$, and $a_{em}$ are complex functions of the relative permittivity $\varepsilon_2$, relative permeability $\mu_2$, and chirality parameter $\kappa$. Setting the chiral polarizability $a_{em} = 0$ recovers the behavior to an achiral particle. One can derive the polarizabilities $a_{ee}$, $a_{mm}$, and $a_{em}$ for the spherical chiral particle from its Mie scattering coefficients. Following the notations of Bohren and Huffman [23], the corresponding Mie scattering coefficients expressed in terms of vector spherical wave functions are defined as

$$\begin{aligned} a_n &= \frac{V_n(R)A_n(L) + V_n(L)A_n(R)}{W_n(L)V_n(R) + W_n(R)V_n(L)},\\ b_n &= \frac{W_n(L)B_n(R) + W_n(R)B_n(L)}{W_n(L)V_n(R) + W_n(R)V_n(L)},\\ c_n &= i\frac{W_n(R)A_n(L) - W_n(L)A_n(R)}{W_n(L)V_n(R) + W_n(R)V_n(L)}, \end{aligned} \tag{4}$$

with

$$\begin{aligned} W_n(J) &= m\psi_n(m_J x)\xi_n'(x) - \xi_n(x)\psi_n'(m_J x),\\ V_n(J) &= \psi_n(m_J x)\xi_n'(x) - m\xi_n(x)\psi_n'(m_J x),\\ A_n(J) &= m\psi_n(m_J x)\psi_n'(x) - \psi_n(x)\psi_n'(m_J x),\\ B_n(J) &= \psi_n(m_J x)\psi_n'(x) - m\psi_n(x)\psi_n'(m_J x). \end{aligned} \tag{5}$$

Here $J$ is $L$ or $R$ and $x = k_1 a$; $\psi_n(\rho) = \rho j_n(\rho)$, $\xi_n(\rho) = \rho h_n^{(1)}(\rho)$ with $j_n(\rho)$ being the spherical Bessel functions and $h_n^{(1)}(\rho)$ being the spherical Hankel functions of the first kind; the relative refractive indices $m_L$, $m_R$ and the mean refractive index $m$ take expressions of $m_L = (\sqrt{\varepsilon_2\mu_2} + \kappa)/\sqrt{\varepsilon_1\mu_1}$, $m_R = (\sqrt{\varepsilon_2\mu_2} - \kappa)/\sqrt{\varepsilon_1\mu_1}$, and $m = (m_L + m_R)/2$, respectively. Within the small particle limit, we retain only the term of $n = 1$ and then obtain the polarizabilities of the dipolar chiral particle as

$$\alpha_{ee} = \frac{i6\pi\varepsilon_1\varepsilon_0}{k_1^3}a_1, \quad \alpha_{mm} = \frac{i6\pi\mu_1\mu_0}{k_1^3}b_1, \quad \alpha_{em} = \frac{6\pi n_1}{ck_1^3}c_1. \tag{6}$$

Substituting Eq. (3) into Eq. (2), the expression of the optical force can be written as

$$\begin{aligned} \langle \mathbf{F} \rangle = {} & \nabla\langle U\rangle + \frac{\sigma n_1}{c}\langle \mathbf{S}\rangle - \mathrm{Im}[\alpha_{em}]\nabla\times\langle \mathbf{S}\rangle - \frac{c\sigma_e}{n_1}\nabla\times\langle \mathbf{L}_e\rangle\\ & - \frac{c\sigma_m}{n_1}\nabla\times\langle \mathbf{L}_m\rangle + \omega\gamma_e\langle \mathbf{L}_e\rangle + \omega\gamma_m\langle \mathbf{L}_m\rangle\\ & + \frac{ck_1^4}{12\pi n_1}\mathrm{Im}[\alpha_{ee}\alpha_{mm}^*]\mathrm{Im}[\mathbf{E}\times\mathbf{H}^*], \end{aligned} \tag{7}$$

with the optical potential,

$$\begin{aligned} \langle U\rangle = {} & \tfrac{1}{4}\mathrm{Re}[\alpha_{ee}]|\mathbf{E}|^2 + \tfrac{1}{4}\mathrm{Re}[\alpha_{mm}]|\mathbf{H}|^2\\ & + \tfrac{1}{2}\mathrm{Re}[\alpha_{em}]\mathrm{Im}[\mathbf{E}\cdot\mathbf{H}^*], \end{aligned} \tag{8}$$

the time-averaged Poynting vector and SAM densities,

$$\begin{aligned} \langle \mathbf{S}\rangle &= \frac{1}{2}\mathrm{Re}[\mathbf{E}\times\mathbf{H}^*],\\ \langle \mathbf{L}_e\rangle &= -\frac{\varepsilon_1\varepsilon_0}{4\omega}\mathrm{Im}[\mathbf{E}\times\mathbf{E}^*],\\ \langle \mathbf{L}_m\rangle &= -\frac{\mu_1\mu_0}{4\omega}\mathrm{Im}[\mathbf{H}\times\mathbf{H}^*], \end{aligned} \tag{9}$$

and the cross sections:

$$\begin{aligned} \sigma_e &= \frac{k_1\mathrm{Im}[\alpha_{ee}]}{\varepsilon_1\varepsilon_0}, \quad \sigma_m = \frac{k_1\mathrm{Im}[\alpha_{mm}]}{\mu_1\mu_0},\\ \sigma &= \sigma_e + \sigma_m - \frac{c^2k_1^4}{6\pi n_1^2}(\mathrm{Re}[\alpha_{ee}\alpha_{mm}^*] + \alpha_{em}\alpha_{em}^*),\\ \gamma_e &= 2\omega\mathrm{Im}[\alpha_{em}] - \frac{ck_1^4}{3\pi\varepsilon_1\varepsilon_0 n_1}\mathrm{Re}[\alpha_{ee}\alpha_{em}^*],\\ \gamma_m &= 2\omega\mathrm{Im}[\alpha_{em}] - \frac{ck_1^4}{3\pi\mu_1\mu_0 n_1}\mathrm{Re}[\alpha_{mm}\alpha_{em}^*]. \end{aligned} \tag{10}$$

In the optical force (7), the first term corresponds to the gradient force $\mathbf{F}_{\mathrm{grad}}$ due to the particle-field interaction; the second term represents the radiation pressure $\mathbf{F}_{\mathrm{rad}}$ proportional to the time-averaged Poynting vector; the third term denotes the "vortex" force $\mathbf{F}_{\mathrm{vor}}$ determined by the energy flow vortex (the curl of the Poynting vector) and particle chirality ($a_{em}$) [17]; the fourth and fifth terms describe the curl-spin force $\mathbf{F}_{\mathrm{curl}}$ associated with the curl of the SAM densities [32,33]; the sixth and seventh terms are referred to the spin density force $\mathbf{F}_{\mathrm{spin}}$ related to the SAM densities and particle chirality ($a_{em}$); and the last term is associated with the alternating flow $\mathbf{F}_{\mathrm{flow}}$ of the so-called "stored energy" [34]. Clearly, the vortex force $\mathbf{F}_{\mathrm{vor}}$ and the spin-density force $\mathbf{F}_{\mathrm{spin}}$ vanish for a dipolar particle without chirality ($a_{em} = 0$).

### B. Tight focusing of vector beams

In optical trapping and manipulation, the optical fields interacting with the target particles are actually the fields of some illumination focused by a high numerical aperture (NA) objective lens. Here, we introduce a vector beam consisting of radial and azimuthal components and having a $\pi/2$ phase difference between the two components as the illumination. Then, the input field at the entrance pupil plane can be written as

$$\mathbf{A}_0(\theta,\phi) = l(\theta)(\cos\phi_0\mathbf{e}_\rho + i\sin\phi_0\mathbf{e}_\phi), \tag{11}$$

which is described in the cylindrical coordinates and uses the relationship of $\rho = f\sin\theta$ in the context of an aplanatic lens with $f$ being the focal length; $\mathbf{e}_\rho$ and $\mathbf{e}_\phi$ are the unit vectors in the radial and azimuthal direction, respectively; angle $\phi_0$ is the polarization angle between the electric vector and the radial vector; $l(\theta)$ is the amplitude function assumed to have a simple form $l(\theta) = l_0$ when $0 \leqslant \theta \leqslant \theta_m$ and $l(\theta) = 0$ otherwise, where $l_0$ is a constant factor dependent on the power of the incident field and $\theta_m$ is the maximal converging angle determined by the NA. After being focused, the focused electric field in the vicinity of the focus, according to the Richards-Wolf vectorial diffraction method [35,36], can be expressed as

$$\mathbf{E}(\mathbf{r}) = \frac{-ik_1 f}{2\pi}\int_0^{\theta_m}\int_0^{2\pi}\mathbf{A}(\theta,\phi)\exp(i\mathbf{k}_1\cdot\mathbf{r})\sin\theta d\phi d\theta, \tag{12}$$

where vectors $\mathbf{k}_1$ and $\mathbf{r}$, separately, designate the wave vector and the observation point position in the image space; integral kernel $\mathbf{A}(\theta,\phi)$ stands for the apodized field which is related to the input field $\mathbf{A}_0(\theta,\phi)$ with the following transform rule [37]:

$$\mathbf{A}(\theta,\phi) = (\cos\theta)^{1/2}\begin{bmatrix}\mathbf{e}_\theta & 0\\ 0 & \mathbf{e}_\phi\end{bmatrix}\begin{pmatrix}A_{0\rho}\\ A_{0\phi}\end{pmatrix}, \tag{13}$$

where $(\mathbf{e}_\theta, \mathbf{e}_\phi)$ are the respective unit vectors in the $\theta$ and $\phi$ directions and $(A_{0\rho}, A_{0\phi})$ are the radial and azimuthal components of the input field $\mathbf{A}_0(\theta,\phi)$. Integrating over the azimuthal direction in Eq. (12) yields the three electric-field components $(E_\rho, E_\phi, E_z)$ in cylindrical coordinates $(\rho_s, \phi_s, z_s)$ as

$$\begin{aligned}
E_\rho &= \cos\phi_0 C\int_0^{\theta_m}\cos^{1/2}\theta\sin(2\theta)l(\theta)e^{ik_1 z_s\cos\theta}J_1(\beta)d\theta,\\
E_\phi &= 2\sin\phi_0 Ci\int_0^{\theta_m}\cos^{1/2}\theta\sin\theta l(\theta)e^{ik_1 z_s\cos\theta}J_1(\beta)d\theta,\\
E_z &= 2\cos\phi_0 Ci\int_0^{\theta_m}\cos^{1/2}\theta\sin^2\theta l(\theta)e^{ik_1 z_s\cos\theta}J_0(\beta)d\theta,
\end{aligned} \tag{14}$$

where $C = k_1 f/2$, $\beta = k_1\rho_s\sin\theta$, and $J_m(\beta)$ is the $m$ th-order Bessel function of the first kind. It is observed that the radial-field component has a $\pi/2$ phase difference with both the azimuthal and axial components. In combination with the SAM density (9), it is clearly seen that the focused field carries not only the longitudinal but also azimuthal SAM densities. A chiral particle trapped in such a focused field is expected to experience an azimuthal optical force through contributions of both the spin-density and curl-spin force terms from the optical force (7). Moreover, the focused field obviously has the same intensity distribution with a general cylindrical vector beam [38]; a hollowlike focusing distribution can be obtained with the polarization angle $0 < \phi_0 < \pi/2$ . In the following calculation, we focused on the case of $\phi_0 = \pi/3$.

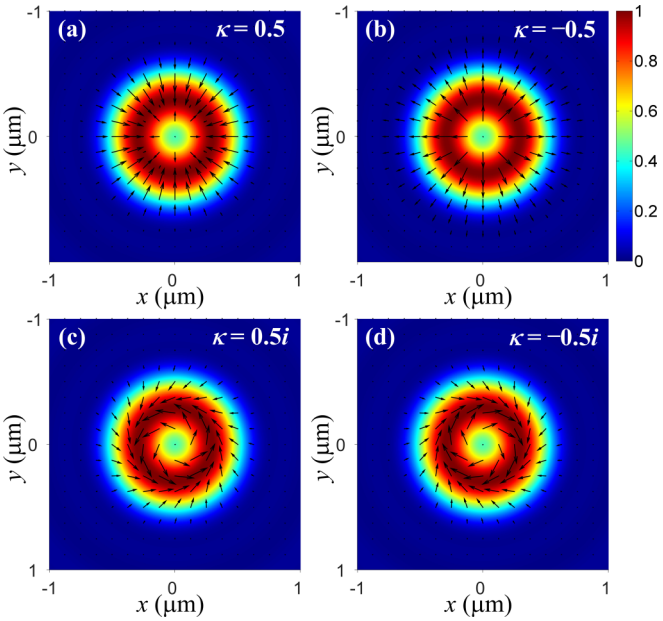


FIG. 1. Transverse optical force distributions experienced by the particle with chirality parameters $\kappa = 0.5$ (a), $-0.5$ (b), $0.5i$ (c), and $-0.5i$ (d), respectively, in the focal plane illuminated by the focused vector beam.

## III. RESULTS AND DISCUSSION

Based on the optical force obtained from the dipole approximation, we can evaluate the force precisely and analyze its dependence on the particle chirality in such a focused vector beam. In what follows, we assume that the input power $P = 100\,\text{mW}$, the free-space wavelength $\lambda_0 = 1.064\,\mu\text{m}$, the objective lens NA $= 1.26$, the refractive index $n_1 = 1.33$, and relative permeability $\mu_1 = 1$ of the image space; the dipolar particle has the radius of $a = 40\,\text{nm}$, relative permittivity $\varepsilon_2 = 2.5$, and permeability $\mu_2 = 1$. Here, the axial equilibrium position is assumed to be in the focal plane and only the transverse trapping is considered. Figures 1(a)–1(d) show the transverse optical force distributions exerted on the chiral particle in the focal plane for the vector beam illumination, where the arrows denote the direction and magnitude of the transverse optical force and the background presents the intensity distribution of the focused field. When the chirality parameter $\kappa = 0.5$ or $-0.5$, the particle experiences only the radial optical force. The radial optical force vanishes on a circle somewhat smaller than that of the intensity maximum for the case of $\kappa = 0.5$ as shown in Fig. 1(a), implying a stable transverse trapping at the off-focus equilibrium position. This is different from an achiral particle that will be trapped on the intensity maxima [39–41]. For the particle with $\kappa = -0.5$ as shown in Fig. 1(b), the radial optical force is always

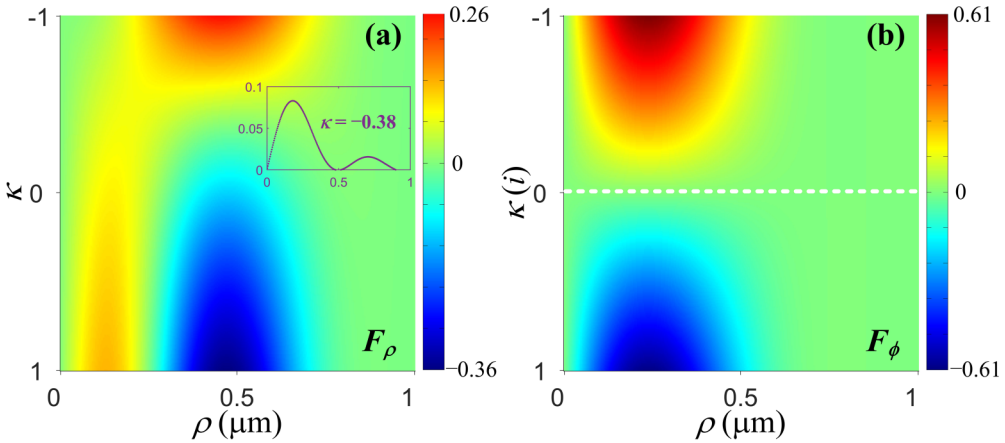


FIG. 2. The radial (a) and azimuthal (b) optical forces as functions of the particle's radial displacement and chirality parameter. The inset shown in (a) is line scan of radial optical force with particle chirality parameter $\kappa = -0.38$ along the radial direction. Both the optical forces are in units of piconewtons.

positive for arbitrary positions and, thus, will push the chiral particle away, manifesting as a nontrap phenomenon in the transverse plane. However, it is dramatically different for the case of $\kappa = 0.5i$ or $-0.5i$ as visualized in Fig. 1(c) or 1(d). The particle experiences a strong azimuthal optical force in addition to the radial optical force near the intensity maxima, indicating that the particle will be trapped off focus on a circle and undergo an orbital motion around the optical axis. With $\kappa = 0.5i$, the orbital motion is in a counterclockwise sense around the negative $z$ axis, whereas for $\kappa = -0.5i$, the orbital motion reverses the direction. According to the focused field (14), there is neither intensity gradient nor wave propagation in the azimuthal direction; thus this azimuthal optical force can also be called the lateral optical force. The formation of this lateral optical force will be analyzed in detail later on.

Figure 2 shows the radial $F_\rho$ and azimuthal $F_\phi$ optical forces as functions of the particle's radial displacement $\rho$ and chirality parameter $\kappa$ (purely real or imaginary value here) for the vector beam illumination. It is clear in Fig. 2(a) that the acquisition of transversely stable trapping is conditional. There exists a critical chirality parameter $\kappa_0(= -0.38)$ in which the transversely off-focus stable trapping position just appears as the curve shown in the inset in Fig. 2(a). To be specific, the radial optical force tends to trap the chiral particles with the chirality parameter $\kappa > \kappa_0$ in a circle near the intensity maxima, while pushing the chiral particles with $\kappa < \kappa_0$ away, manifesting as a nontrap phenomenon. As a consequence, the chiral particles with different magnitudes of chirality can be separated, thus possibly implementing sorting of the chiral particles. Both the sign and magnitude of the azimuthal optical force are directly related to the particle chiral absorption which expresses itself as the imaginary part of the chirality parameter, as shown in Fig. 2(b). The magnitude of the azimuthal optical force increases with the increase of the magnitude of the chiral absorption. If the chiral absorption is positive, the azimuthal optical force is negative, and vice versa, resulting in a negative or positive orbiting motion of the chiral particles, and the azimuthal optical force vanishes when the particle is without chiral absorption, as denoted by the white dashed line. Therefore, we conclude that the focused vector beam can selectively trap the chiral particles with different real chirality parameters, and even selectively rotate the chiral particle with different imaginary chirality parameters, leading to an optical chirality sorting of the chiral particles in the transverse plane.

Next, we turn to the cases of chiral particles with complex chirality parameters, $\kappa = \mathrm{Re}(\kappa) + i\mathrm{Im}(\kappa)$. Figure 3 presents the changes of radial $F_\rho$ and azimuthal $F_\phi$ optical forces of the chiral particles suffered along the radial direction with a variety of chirality parameters. When $\mathrm{Im}(\kappa)$ is fixed at 0.2, the radial optical force $F_\rho$ varies greatly with $\mathrm{Re}(\kappa)$ as shown in Fig. 3(a). With $\mathrm{Re}(\kappa)$ increasing from $-0.8$ to 0.8, the particle also experiences a process of being pushed away and trapped off axis on a circle. The stiffness of the radial trapping increases with the value of $\mathrm{Re}(\kappa)$ increasing, indicating an easier transverse trapping will be achieved. Moreover, the transverse trapped equilibrium position of the particle is closer and closer to the optical axis. While with $\mathrm{Im}(\kappa)$ changing from $-0.8$ to 0.8 when $\mathrm{Re}(\kappa)$ is held at 0.2 as shown in Fig. 3(b), the changes of the $F_\rho$ are small, and nearly no change of the $F_\rho$ can be discerned with the positive and negative $\mathrm{Im}(\kappa)$ by comparing the curves of $\kappa = 0.2 - 0.8i(0.2 - 0.4i)$ and $\kappa = 0.2 + 0.8i(0.2 + 0.4i)$. Consequently, the real part of the chirality parameter has a more significant effect than the imaginary part on the radial optical force. Nevertheless, for the azimuthal optical force $F_\phi$, the situation is remarkably different. With $\mathrm{Re}(\kappa)$ increasing, as illustrated in Fig. 3(c), the $F_\phi$ decreases, indicating that the real part of the chirality parameter can be appropriately reduced to obtain an enhanced orbital motion of the chiral particle. Notice from Fig. 3(d) that the $F_\phi$ also vanishes with $\mathrm{Im}(\kappa) = 0$ even though $\mathrm{Re}(\kappa)$ is 0.2. The increase of the absolute value of $\mathrm{Im}(\kappa)$ results in an obvious enhancement of the $F_\phi$. In addition, the sign of the $F_\phi$ is determined by the sign of $\mathrm{Im}(\kappa)$, becoming negative (positive) for positive (negative) values of $\mathrm{Im}(\kappa)$. Therefore, for the particle with complex chirality parameter, the real and imaginary parts of the chirality parameter are also the decisive factors for realizing the transverse trapping and orbital rotation, respectively.

Of course, to obtain an orbital rotation for particles with a complex chirality parameter, the particles must first be trapped transversely. Since this is so, the critical chirality parameter

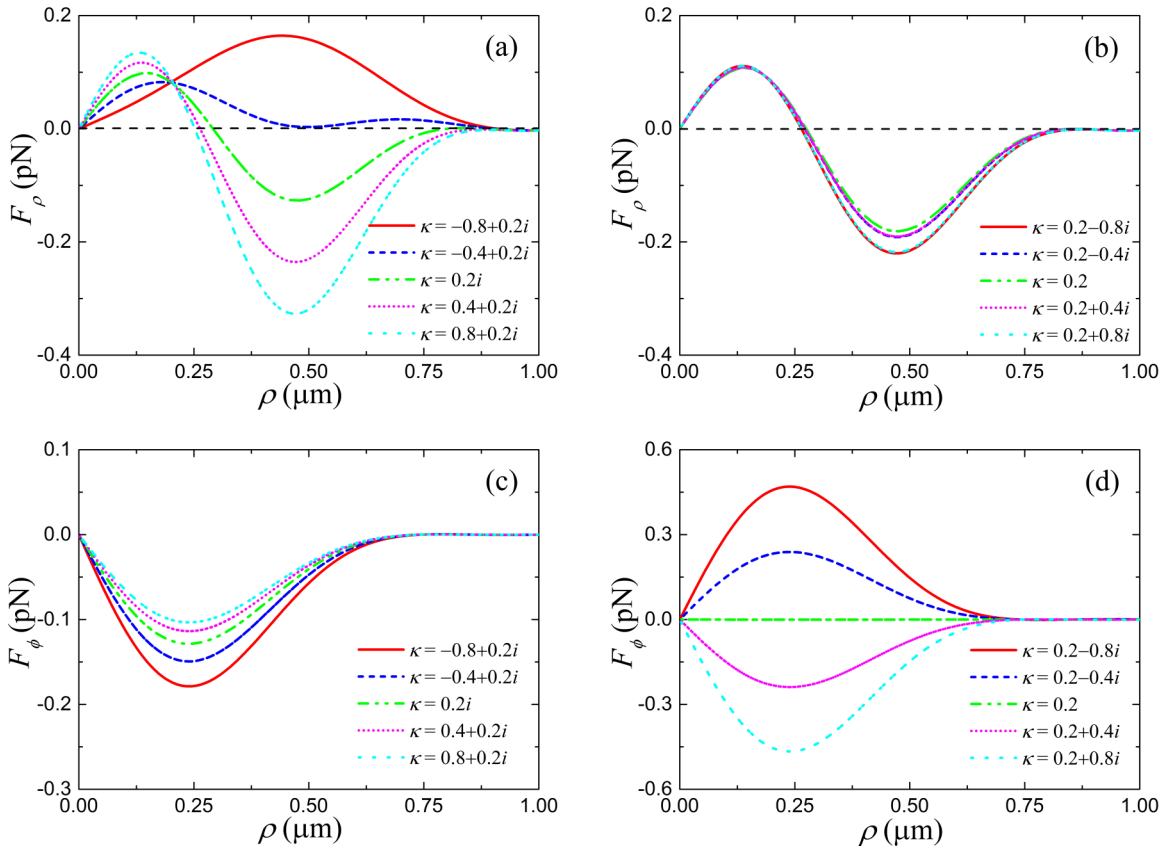


FIG. 3. The radial (a,b) and azimuthal (c,d) optical forces on the chiral particle with different chirality parameters under the vector beam illumination.

for particles being trapped transversely will also be a complex value and may be changed. To show this, the dependence of the real part $\mathrm{Re}(\kappa_0)$ of the critical chirality parameter on the particles' chiral absorption $\mathrm{Im}(\kappa)$ are examined in Fig. 4. That is, the particles with a certain chiral absorption that can be trapped transversely should satisfy the condition of the chirality parameter, $\mathrm{Re}(\kappa) > \mathrm{Re}(\kappa_0)$. Since the size of the particles has a certain influence on the magnitude of the optical force, the cases of particles with radii of 20 and 30 nm

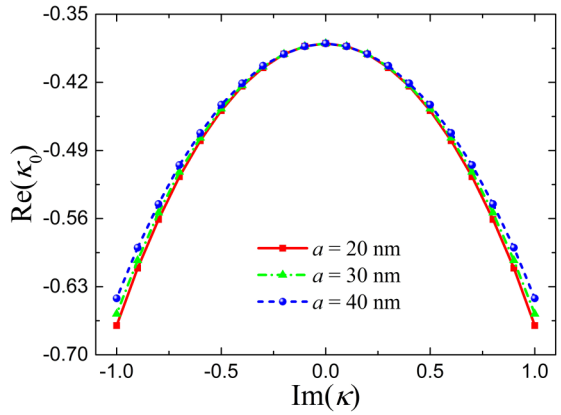


FIG. 4. Changes of the real part of the critical chirality parameters for particles with the chiral absorption to be trapped transversely under the vector beam illumination for different particles' radii.

are also plotted as comparisons. Obviously, the curves of $\mathrm{Re}(\kappa_0)$ show the same variation tendency and are even functions of $\mathrm{Im}(\kappa)$. The values of $\mathrm{Re}(\kappa_0)$ increase with the particle size increasing; the differences in $\mathrm{Re}(\kappa_0)$ for the three radii become smaller and smaller as $|\mathrm{Im}(\kappa)|$ decreases and finally vanish at $\mathrm{Im}(\kappa) = 0$. Furthermore, with increasing the values of $\mathrm{Im}(\kappa)$, $\mathrm{Re}(\kappa_0)$ first increases until a peak of $-0.38$ is reached at $\mathrm{Im}(\kappa) = 0$; thereafter it decreases. This facilitates the further sorting of the chiral particles with different radii and complex chirality parameters. Figure 4 also suggests that the particles with $\mathrm{Re}(\kappa) > -0.38$ can be trapped transversely in such a focused vector beam, irrespective of the chiral absorption.

The aforementioned discussions prove that such a focused vector field can selectively trap and rotate chiral particles by the chirality-tailored radial and azimuthal (lateral) optical forces, respectively. To trace the physical origins of these transverse optical forces on the chiral particles, the contribution of each term of the optical forces in Eq. (7) to the radial $F_\rho$ and azimuthal $F_\phi$ optical forces under the vector beam illumination is plotted in Fig. 5, where the chirality parameter $\kappa = 0.5 + 0.5i$. In Fig. 5(a), it can be seen that the $F_\rho$ overwhelmingly comes from the gradient force $F_{\mathrm{grad}}$, arising from the interaction of particle polarizabilities ($a_{ee}$, $a_{mm}$, $a_{em}$) with the electric $|\mathbf{E}|^2$ and magnetic $|\mathbf{H}|^2$ energy densities as well as chirality density $\mathrm{Im}[\mathbf{E} \cdot \mathbf{H}^*]$. However, the $F_\phi$ in Fig. 5(b) is dominated largely by the spin-density force $F_{\mathrm{spin}}$ and the vortex force $F_{\mathrm{vor}}$ which is directly related to the particle chirality

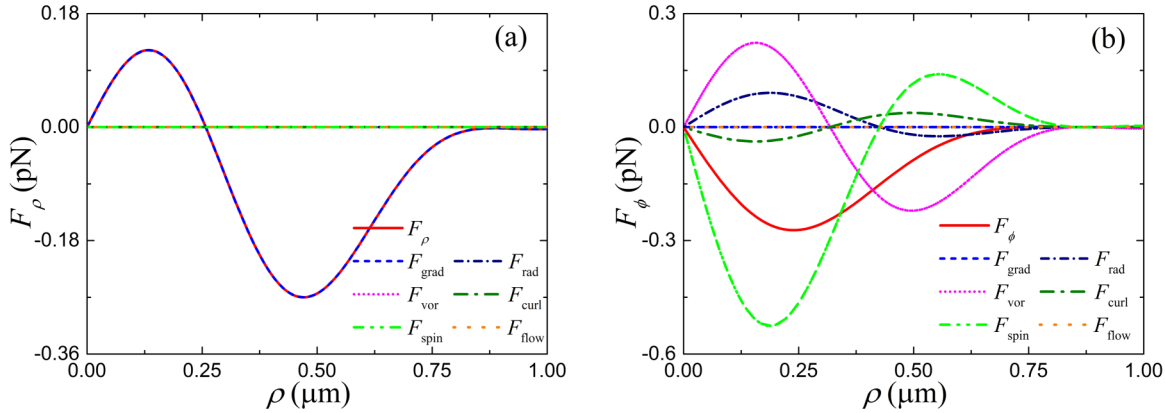


FIG. 5. The contributions of decomposed radial (a) and azimuthal (b) optical forces defined in Eq. (7) acting on the chiral particle with $\kappa = 0.5 + 0.5i$ under the vector beam illumination.

($a_{em}$), also associated with the radiation pressure $\mathbf{F}_{\text{rad}}$ and the curl-spin force $F_{\text{curl}}$, but almost not related to the gradient force and the alternating flow owing to the terms of $\nabla\langle U\rangle$ and $\text{Im}[\mathbf{E}\times\mathbf{H}^*]$ without the azimuthal component. As a result, the lateral optical force caused by the tightly focused field in our case originates from a complex process consisting of four force terms, differing from all those reported previously [17–22]. Such lateral optical force–induced orbital motion of the chiral particle is derived from the transformation of optical SAM of the focused field into the mechanical orbital angular momentum (OAM) of the particle, the curl of the Poynting vector and SAM, as well as the radiation pressure. It becomes clear that, in addition to the usual optical gradient force and radiation pressure as well as curl-spin force, the chiral particle indeed can be affected by new forces which directly depend on the particle chirality.

Finally, the dependences of the above contributing optical force terms on the particle chirality parameter are further investigated. In Fig. 5(a), following the optical potential of Eq. (8), the gradient force $F_{\text{grad}}$ can be subdivided into three

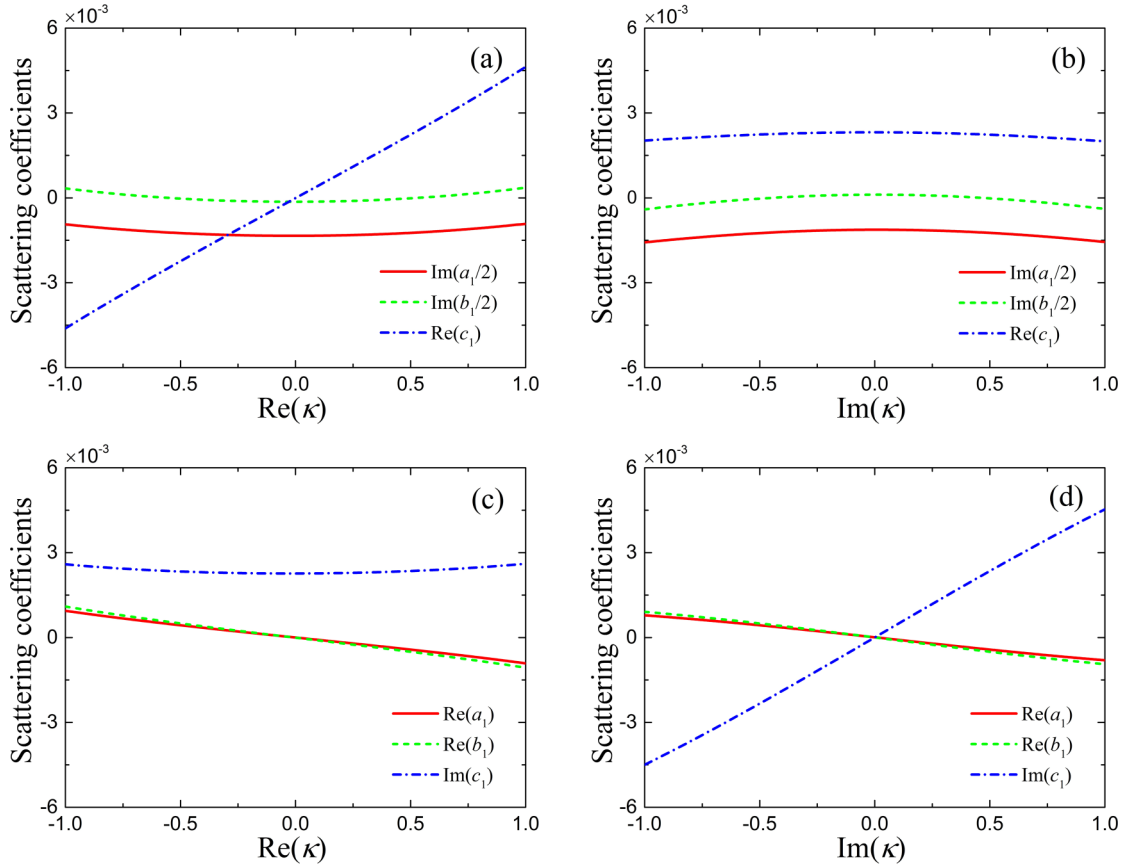


FIG. 6. The scattering coefficients involved in the radial (a,b) and azimuthal (c,d) optical forces as functions of particle chirality parameter $\text{Re}(\kappa)$ and $\text{Im}(\kappa)$ under the vector beam illumination. Fix $\text{Im}(\kappa) = 0.5$ in (a,c) and $\text{Re}(\kappa) = 0.5$ in (b,d).

parts and expressed in the form with only electric field $\mathbf{E}$ based on the Maxwell equation of $\nabla \times \mathbf{E} = -\partial \mathbf{B}/\partial t$. Thus, for a given incident field, different factors related to the scattering coefficients involved in these three parts are, separately, $\mathrm{Im}(a_1/2)$, $\mathrm{Im}(b_1/2)$, and $\mathrm{Re}(c_1)$. Figures 6(a) and 6(b) plot these scattering coefficients as functions of the real $\mathrm{Re}(\kappa)$ and imaginary $\mathrm{Im}(\kappa)$ parts of the chirality parameter, respectively. Clearly, the coefficients $\mathrm{Im}(a_1/2)$ and $\mathrm{Im}(b_1/2)$ are much less sensitive to the magnitude and sign of the chirality parameter, whereas the coefficient $\mathrm{Re}(c_1)$ changes greatly with $\mathrm{Re}(\kappa)$ exhibiting a nearly linear dependence on $\mathrm{Re}(\kappa)$ and is also insensitive to $\mathrm{Im}(\kappa)$. Consequently, it once again proves that the real part of the chirality parameter has more influence on the radial optical force, and also shows that the appearance of trap and nontrap states of the chiral particles are due to the opposite signs of coefficient $\mathrm{Re}(c_1)$ for opposite $\mathrm{Re}(\kappa)$.Concerning Fig. 5(b), likewise, the four force terms contributing to the azimuthal optical force are separately related to different factors that are associated with the scattering coefficients for the same incident field. Specifically, the spin density force $F_{\mathrm{spin}}$ is related to the coefficients $\mathrm{Im}(c_1 + a_1 c_1^*)$ and $\mathrm{Im}(c_1 + b_1 c_1^*)$, the vortex force $F_{\mathrm{vor}}$ to $\mathrm{Im}(c_1)$, the radiation pressure $F_{\mathrm{rad}}$ to $\mathrm{Re}(a_1 + b_1 - a_1 b_1^*) + c_1 c_1^*$, and the curl-spin force $F_{\mathrm{curl}}$ to $\mathrm{Re}(a_1/2)$ and $\mathrm{Re}(b_1/2)$. Notice that the coefficients $\mathrm{Im}(a_1 c_1^*)$ and $\mathrm{Im}(b_1 c_1^*)$ are much smaller than the $\mathrm{Im}(c_1)$, and the $\mathrm{Re}(a_1 b_1^*) + c_1 c_1^*$ is much smaller than the $\mathrm{Re}(a_1)$ or $\mathrm{Re}(b_1)$. As a result, the azimuthal optical force is mainly determined by the scattering coefficients of $\mathrm{Im}(c_1)$, $\mathrm{Re}(a_1)$, and $\mathrm{Re}(b_1)$. Changes of these coefficients with the real $\mathrm{Re}(\kappa)$ and imaginary $\mathrm{Im}(\kappa)$ parts of the chirality parameter are shown in Figs. 6(c) and 6(d), respectively. Evidently, except for the $\mathrm{Im}(c_1)$ exhibiting an almost symmetric behavior with respect to the sign of $\mathrm{Re}(\kappa)$, the other five curves depend nearly linearly on the chirality parameter. The values of coefficient $\mathrm{Im}(c_1)$ with the chirality parameter varied are much larger compared to those of coefficients $\mathrm{Re}(a_1)$ and $\mathrm{Re}(b_1)$. This leads to the force terms associated with the $\mathrm{Im}(c_1)$ having greater influences on the azimuthal optical force, as mentioned above. Moreover, the $\mathrm{Im}(c_1)$ is insensitive to $\mathrm{Re}(\kappa)$ but takes opposite signs for opposite $\mathrm{Im}(\kappa)$. Accordingly, the sign of the azimuthal optical force is determined by the sign of the chiral absorption, while the magnitude is mainly determined by the chiral absorption but also related to the real part of the chirality parameter.

## IV. CONCLUSION

In summary, we have numerically shown that the tightly focused vector beam can induce different transverse optical forces on the dipolar chiral particles with different chirality, achieving an effective optical sorting of the chiral particles. The radial optical force, resulting from the gradient force associated with the particle-field interaction, is sensitive to both the sign and magnitude of the real part of the chirality parameter, and tends to trap the chiral particles with $\mathrm{Re}(\kappa) > \mathrm{Re}(\kappa_0)$ ($\kappa_0$ is the critical chirality parameter) on a circle while pushing the particles with $\mathrm{Re}(\kappa) < \mathrm{Re}(\kappa_0)$ away, enabling a selective trapping of the chiral particles in the transverse plane. The lateral optical force manifests itself as the azimuthal optical force, arising from the transformation of optical SAM of the focused field into the mechanical OAM of the particle and the curl of the Poynting vector and SAM, as well as the radiation pressure, which is sensitive to both the sign and magnitude of the chiral absorption. This can induce an orbital rotation of the trapped chiral particles around the negative optical axis with $\mathrm{Im}(\kappa) > 0$ but around the positive optical axis with $\mathrm{Im}(\kappa) < 0$, leading to a selective separation of the chiral particles. The results of chirality-controlled optical trapping and manipulation may provide a possible route toward optical identification and separation of chiral particles.

## ACKNOWLEDGMENTS

This research is supported by the Natural Science Foundation of China (NSFC) under Grants No. 11474352, No. 81427802 and No. 11574389, and the National Basic Research Program (973 Program) of China under Grant No. 2012CB921900.

[1] A. Guijarro and M. Yus, *The Origin of Chirality in the Molecules of Life: A Revision from Awareness to the Current Theories and Perspectives of this Unsolved Problem* (Royal Society of Chemistry, Cambridge, 2008).

[2] L. A. Nguyen, H. He, and C. Pham-Huy, Chiral drugs: An overview, Int. J. Biomed. Sci. **2**, 85 (2006).

[3] C. M. Dobson, Protein folding and misfolding, Nature **426**, 884 (2003).

[4] H. Caner, E. Groner, L. Levy, and I. Agranat, Trends in the development of chiral drugs, Drug Discovery Today **9**, 105 (2004).

[5] S. W. Smith, Chiral toxicology: It's the same thing … only different, Toxicol. Sci. **110**, 4 (2009).

[6] B. S. Sekhon, Chiral pesticides, J. Pestic. Sci. **34**, 1 (2009).

[7] Y. Zhao, A. A. Saleh, and J. A. Dionne, Enantioselective optical trapping of chiral nanoparticles with plasmonic tweezers, ACS Photonics **3**, 304 (2016).

[8] L. Carretero, P. Acebal, and S. Blaya, Chiral Rayleigh particles discrimination in dynamic dual optical traps, J. Quant. Spectrosc. Radiat. Transfer **201**, 209 (2017).

[9] G. Tkachenko and E. Brasselet, Optofluidic sorting of material chirality by chiral light, Nat. Commun. **5**, 3577 (2014).

[10] A. Canaguier-Durand, J. A. Hutchison, C. Genet, and T. W. Ebbesen, Mechanical separation of chiral dipoles by chiral light, New J. Phys. **15**, 123037 (2013).

[11] D. S. Bradshaw and D. L. Andrews, Chiral discrimination in optical trapping and manipulation, New J. Phys. **16**, 103021 (2014).

[12] H. Chen, C. Liang, S. Liu, and Z. Lin, Chirality sorting using two-wave-interference-induced lateral optical force, Phys. Rev. A **93**, 053833 (2016).

[13] Y. Zhao, A. N. Askarpour, L. Sun, J. Shi, X. Li, and A. Alù, Chirality detection of enantiomers using twisted optical metamaterials, Nat. Commun. **8**, 14180 (2017).

[14] D. S. Bradshaw and D. L. Andrews, Laser optical separation of chiral molecules, Opt. Lett. **40**, 677 (2015).
[15] T. Cao and Y. Qiu, Lateral sorting of chiral nanoparticles using Fano-enhanced chiral force in visible region, Nanoscale **10**, 566 (2018).
[16] W. Lu, H. Chen, S. Guo, S. Liu, and Z. Lin, Selectively transporting small chiral particles with circularly polarized Airy beams, Opt. Lett. **43**, 2086 (2018).
[17] S. B. Wang and C. T. Chan, Lateral optical force on chiral particles near a surface, Nat. Commun. **5**, 3307 (2014).
[18] F. J. Rodríguez-Fortuño, N. Engheta, A. Martínez, and A. V. Zayats, Lateral forces on circularly polarizable particles near a surface, Nat. Commun. **6**, 8799 (2015).
[19] A. Hayat, J. P. B. Mueller, and F. Capasso, Lateral chirality-sorting optical forces, Proc. Natl. Acad. Sci. USA **112**, 13190 (2015).
[20] F. Kalhor, T. Thundat, and Z. Jacob, Universal spin-momentum locked optical forces, Appl. Phys. Lett. **108**, 061102 (2016).
[21] T. Cao, L. Mao, D. Gao, W. Ding, and C.-W. Qiu, Fano resonant $Ge_2Sb_2Te_5$ nanoparticles realize switchable lateral optical force, Nanoscale **8**, 5657 (2016).
[22] T. Zhang, M. R. C. Mahdy, Y. Liu, J. H. Teng, C. T. Lim, Z. Wang, and C.-W. Qiu, All-optical chirality-sensitive sorting via reversible lateral forces in interference fields, ACS Nano **11**, 4292 (2017).
[23] C. F. Bohren and D. R. Huffman, *Absorption and Scattering of Light by Small Particles* (John Wiley & Sons, New York, 1983).
[24] I. V. Lindell, A. H. Sihvola, S. A. Tretyakov, and A. J. Viitanen, *Electromagnetic Waves in Chiral and Bi-Isotropic Media* (Artech House, Boston, 1994).
[25] A. Lakhtakia, V. K. Varadan, and V. V. Varadan, *Time-Harmonic Electromagnetic Fields in Chiral Media* (Springer-Verlag, New York, 1989).
[26] M. Yokota, S. He, and T. Takenaka, Scattering of a Hermite-Gaussian beam field by a chiral sphere, J. Opt. Soc. Am. A **18**, 1681 (2001).
[27] L. D. Barron, *Molecular Light Scattering and Optical Activity* (Cambridge University Press, Cambridge, 2004).
[28] A. Canaguier-Durand and C. Genet, Chiral route to pulling optical forces and left-handed optical torques, Phys. Rev. A **92**, 043823 (2015).
[29] P. C. Chaumet and A. Rahmani, Electromagnetic force and torque on magnetic and negative-index scatterers, Opt. Express **17**, 2224 (2009).
[30] M. Nieto-Vesperinas, J. J. Sáenz, R. Gómez-Medina, and L. Chantada, Optical forces on small magnetodielectric particles, Opt. Express **18**, 11428 (2010).
[31] J. Chen, J. Ng, Z. Lin, and C. T. Chan, Optical pulling force, Nat. Photonics **5**, 531 (2011).
[32] S. Albaladejo, M. I. Marqués, M. Laroche, and J. J. Sáenz, Scattering Forces from the Curl of the Spin Angular Momentum of a Light Field, Phys. Rev. Lett. **102**, 113602 (2009).
[33] I. Liberal, I. Ederra, R. Gonzalo, and R. W. Ziolkowski, Near-field electromagnetic trapping through curl-spin forces, Phys. Rev. A **87**, 063807 (2013).
[34] J. D. Jackson, *Classical Electrodynamics*, 3rd ed. (John Wiley & Sons, New York, 1999).
[35] B. Richards and E. Wolf, Electromagnetic diffraction in optical systems. II. Structure of the image field in an aplanatic system, Proc. R. Soc. A **253**, 358 (1959).
[36] K. S. Youngworth and T. G. Brown, Focusing of high numerical aperture cylindrical-vector beams, Opt. Express **7**, 77 (2000).
[37] Q. Zhan, Cylindrical vector beams: From mathematical concepts to applications, Adv. Opt. Photonics **1**, 1 (2009).
[38] M. Li, S. Yan, B. Yao, M. Lei, Y. Yang, J. Min, and D. Dan, Intrinsic optical torque of cylindrical vector beams on Rayleigh absorptive spherical particles, J. Opt. Soc. Am. A **31**, 1710 (2014).
[39] D. G. Grier, A revolution in optical manipulation, Nature **424**, 810 (2003).
[40] M. Li, S. Yan, Y. Liang, P. Zhang, and B. Yao, Transverse spinning of particles in highly focused vector vortex beams, Phys. Rev. A **95**, 053802 (2017).
[41] R. Paez-Lopez, U. Ruiz, V. Arrizon, and R. Ramos-Garcia, Optical manipulation using optimal annular vortices, Opt. Lett. **41**, 4138 (2016).